Experimental Investigation of the Three-Dimensional Interaction of a Strong Shock with a Spherical Density Inhomogeneity

H. F. Robey,[1] T. S. Perry,[1] R. I. Klein,[1,2] J. O. Kane,[1] J. A. Greenough,[1] and T. R. Boehly[3]
[1]*Lawrence Livermore National Laboratory, University of California, Livermore, California 94550*
[2]*Department of Astronomy, University of California, Berkeley, California 94720*
[3]*Laboratory for Laser Energetics, University of Rochester, Rochester, New York 14623*
(Received 11 May 2001; revised manuscript received 23 January 2002; published 1 August 2002)

Laser-driven experiments are described which probe the interaction of a very strong shock with a spherical density inhomogeneity. The interaction is viewed from two orthogonal directions enabling visualization of both the initial distortion of the sphere into a double vortex ring structure as well as the onset of an azimuthal instability that ultimately results in the three-dimensional breakup of the ring. The experimental results are compared with 3D numerical simulations and are shown to be in remarkable agreement with the incompressible theory of Widnall *et al.* [J. Fluid Mech. **66**, 35 (1974)].

DOI: 10.1103/PhysRevLett.89.085001 PACS numbers: 52.35.Tc, 52.50.Jm, 52.57.–z

The interaction of a shock wave with a discrete density inhomogeneity is a problem of fundamental interest, which can be used as a building block to develop an understanding of more complicated problems involving the propagation of shocks through random media. An example of such a problem is the interaction of shock waves in the interstellar medium (ISM) such as those associated with supernovae, stellar winds, bipolar flows, and HII regions with interstellar clouds. This interaction is critical to understanding the evolution of the ISM, the mixing of interstellar clouds with the ISM, and the viability of this mechanism for triggered star formation as shown by Klein *et al.* [1,2].

Several previous experimental studies have focused on this problem. Haas and Sturtevant [3] performed shock tube experiments at low Mach number ($M < 1.3$) using both cylindrical as well as spherical density inhomogeneities. Using optical diagnostics, they very clearly visualized the transmitted, reflected, and refracted waves occurring in the interaction, as well as the subsequent deformation of the resulting flow. Klein *et al.* [4] performed similar studies on the Nova laser extending the experiments into the strong shock regime ($M > 10$), which is of interest to the astrophysical application. The primary diagnostic in these experiments was x-ray absorption radiography. In each of these studies, the interaction was viewed from the side (direction perpendicular to that of shock propagation). While a great deal of information can be obtained from this viewpoint, a quantitative understanding of the nonaxisymmetric instability and breakup requires an additional diagnostic view. The present experiments augment these previous studies by simultaneously diagnosing the interaction from two orthogonal views, thereby enabling the full three-dimensional topology of the interaction to be understood.

The experiments are conducted on the Omega laser at the Laboratory for Laser Energetics [5]. Figure 1 shows a three-dimensional view of the target used for the experiments. The target is mounted in a 1500 μm long cylindrical beryllium shock tube, which improves the planarity of the experiment by decreasing lateral expansion of the target materials. Beryllium was used for the shock tube since it is essentially transparent to the diagnostic x rays [6]. The shock tube is filled with polystyrene (CH) at a density of 1.044 g/cm^3. Embedded within this polystyrene cylinder at a depth of 500 μm from the ablation surface is a Cu sphere of diameter 120 ± 2 μm and a density of 8.95 g/cm^3.

The strong shock conditions of interest are achieved by directing ten beams with a nominal measured energy of 500 J/beam, a flat temporal pulse of length of 1 ns, and a laser wavelength of 0.351 μm onto the target. Each individual beam has a super-Gaussian spatial intensity profile defined as $I/I_0 = \exp[-(r/412\ \mu\text{m})]^{4.7}$. The peak intensity of all ten beams was $I_0 = 9 \times 10^{14}$ W/cm^2. The intensity is constant to within 2% over a central diameter of 400 μm and falls off by about 14% at a diameter of 600 μm. A 75 μm thick Be shield with an outer diameter

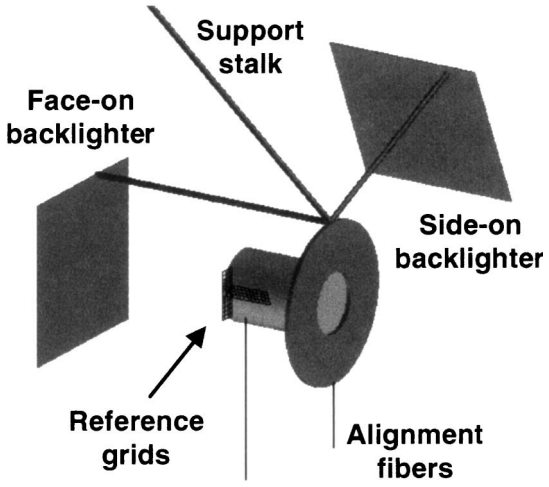

FIG. 1. Three-dimensional view of the target and backlighter configuration.

of 2.5 mm and an inner aperture of 950 μm was used to delay the propagation of a shock around the sides of the target.

Direct-drive laser illumination of the target was used in order to permit the face-on imaging of the interaction. Previous experiments [4] used indirect drive in which the laser energy was directed onto a cylindrical gold hohlraum producing a uniform x-ray flux, which then launched the strong shock. Indirect drive has the disadvantage, however, that the hohlraum fills with optically thick Au plasma blown off from the walls, and this prohibits the late-time imaging of the interaction from the face-on direction. Direct drive, by comparison, maintains face-on diagnostic access for the entire duration of the experiment.

The interaction was diagnosed with 5.2 keV x rays generated by directing an additional eight Omega beams onto each of two nominally orthogonal 12 μm thick vanadium backlighter foils located 4 mm from the center of the target (Fig. 1). These beams, driven by a separate oscillator, were delayed in time relative to the drive beams by up to 39 ns to observe the interaction at late times. The differential absorption of the backlighter x rays by the target materials was imaged with two gated x-ray framing cameras [7], which had a spatial resolution set by a pinhole diameter of 10 μm and a temporal resolution of 200 ps.

Figure 2 shows experimental radiographs of the interaction in both the side-on and face-on directions at $t =$ 13, 26, and 39 ns. In each case, the face-on images are delayed by 2 ns relative to the side-on images. Each time-delayed pair of images is obtained from a separate target and laser shot. Also, for clarity, all face-on images are plotted at twice the magnification of the corresponding side-on images. The spatial location and scale of the resulting structure were determined from reference grids consisting of 5 μm Au wires with a period of 63 μm. Figures 2(a) and 2(b) show images at $t = 13$ and 15 ns of the side-on and the face-on structure, respectively. The shock is clearly seen having just passed over the sphere. From 1D numerical simulations, the shock pressure at the time of impact with the sphere is 12 Mbar and the shock velocity is 25 μm/ns. With the temporal resolution of the diagnostic, this gives a motion blurring of the shock front of 5 μm, which is less than the spatial resolution set by the pinhole. The mean velocity of the shocked Cu at this time is 10 μm/ns, and the ion temperature behind the shock is approximately 10 eV. For a shock of this temperature propagating in low density material ($\sim$5–10 mg/cm^3), there is a possibility of a radiation precursor affecting the temperature of the material ahead of the shock. At the densities of the present experiment, however, this is not an issue.

The shock is curved with a measured radius of curvature of 1 mm. This is due to the nonuniform spatial profile of the initial laser energy deposition. The radius of curvature is much larger than the sphere diameter, however, so the interaction is reasonably approximated as a planar shock. The sphere is compressed in the longitudinal direction with a measured width of 80 μm. The lateral dimension of the sphere remains essentially unchanged at 120 μm. Figure 2(b) shows the corresponding face-on view. In this view, the sphere is seen to be essentially unperturbed, with a diameter that is unchanged from its initial condition.

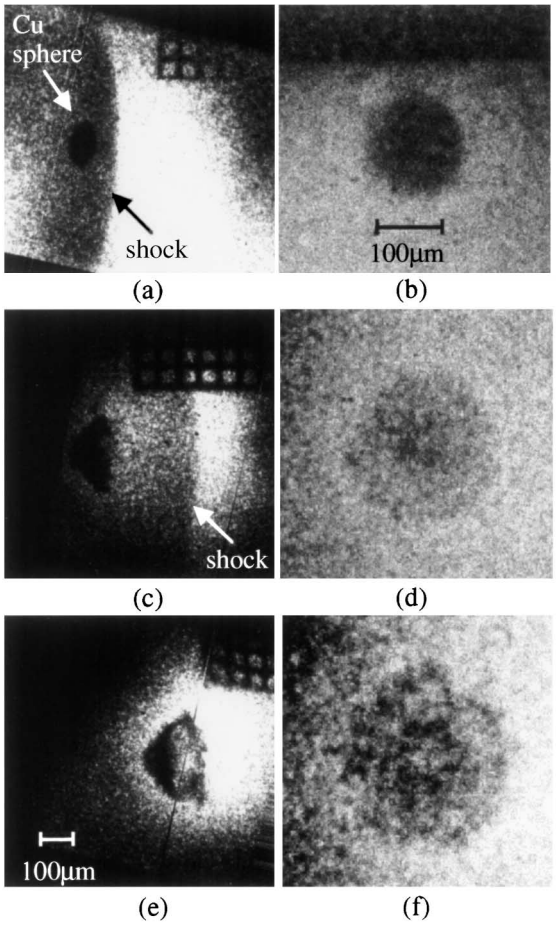

FIG. 2. Side-on (left column) and face-on (right column) radiographs of the shocked sphere at $t = 13$ ns (a),(b), $t =$ 26 ns (c),(d), and $t = 39$ ns (e),(f).

Figures 2(c) and 2(d) show the structure resulting at $t =$ 26 ns and 28 ns, respectively. The shock has now pulled away from the sphere and has become somewhat more planar with an increased radius of curvature of 2 mm. The sphere is now considerably distorted. The corresponding face-on view of Fig. 2(d) shows that there remains a dense core of approximate diameter 70 μm in the center, with a 200 μm diameter surrounding region of lower optical depth, which corresponds to a relatively thin shell of shocked Cu.

Figures 2(e) and 2(f) show the continued distortion at $t = 39$ and 41 ns. The shock has now moved out of the field of view of the diagnostic. The vortical roll-up is clearly seen in the side-on image, and the face-on view now shows a rather distinct double ''ring'' structure. The inner ring, which is the feature of greatest optical depth contrast, exhibits a visible azimuthal mode structure with a mode number of 5. In the center of this ring is a region

of reduced optical depth (or increased transparency). Surrounding the central ring is an outer ring that is significantly modulated in the azimuthal direction.

The face-on image is analyzed quantitatively in Fig. 3. Figure 3(a) shows an additional face-on radiograph from the experiment taken from a slightly different time from that of Fig. 2(f). Figure 3(b) shows an averaged radial lineout of the optical depth modulation obtained from Fig. 3(a). Radial lineouts were taken over azimuthal angles $0 < \theta < 2\pi$ and averaged to form the radial lineout of Fig. 3(b). To increase further the statistical significance, the procedure was repeated for four images each separated in time by $\Delta t = 60$ ps. Beginning at $r = 0$, there is a region of approximately 30–40 μm in radial extent which exhibits a relatively high transparency (low optical depth). At $r \approx 46$ μm, the inner ring is seen with the lowest transparency. The second, outer ring is seen at $r \approx 127$ μm.

The azimuthal mode structure of these two rings is analyzed in Figs. 3(c) and 3(d) by taking radially averaged, azimuthal lineouts at $r = 46 \pm 10$ μm and $127 \pm$ μm. Figure 3(c) agrees with the visual observation of the images in revealing a dominant mode number of 5 for the inner ring. By comparison, Fig. 3(d) shows a higher mode number of 14–16 for the outer ring. The mode number spectra obtained by performing a Fourier transform of the lineouts of Figs. 3(c) and 3(d) are shown in Figs. 3(e) and 3(f). For comparison, the same procedure is used on a region of the face-on image outside of the distorted Cu sphere to obtain a spectrum of the background. For the inner ring, a peak is seen above the background level at a mode number of 5–8. For the outer ring two peaks are seen above the background level, one at a mode number of 5–6 and one at approximately 15. In both cases, the signal-to-background level is low due to the rather poor photon statistics of these images. Though rather poorly resolved with the present diagnostic capability, the observation of the azimuthal structure is robust and has been observed in experiments on three separate occasions, using spheres with initial diameters of 120 and 240 μm.

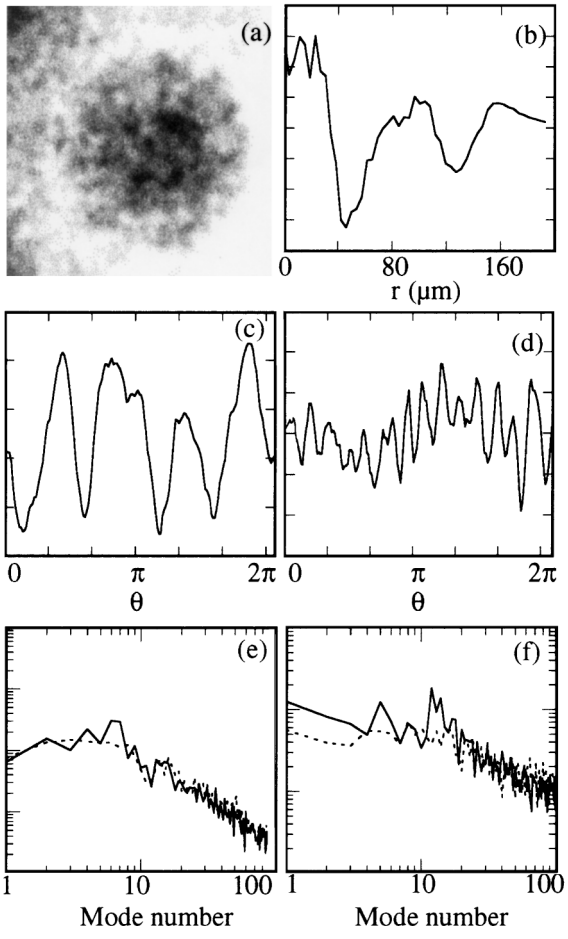

FIG. 3. (a) Face-on radiograph at $t = 41$ ns. (b) Radial lineout through the face-on image. Azimuthal lineout through inner ring at $r = 46$ μm (c) and outer ring at $r = 127$ μm (d). Mode number spectra (e),(f) corresponding to the azimuthal lineouts of (c),(d).

The possibility exists that the observed azimuthal mode structure could have been produced by a nonuniform shock front originating from direct-drive laser imprinting. This is unlikely, however, for two reasons. First, the Cu sphere is located 500 μm from the ablation surface precisely to avoid this possibility. Perturbations to a propagating shock decay in a distance comparable to the perturbation wavelength. Only perturbations greater than several hundred microns will survive to this depth into the target. The observed azimuthal modulation is of order 40 μm, which is too small to be due to laser imprinting. Second, as seen in the face-on images of Figs. 2(b), 2(d), and 2(f), the azimuthal modulations are not seen early in time, but rather develop later consistent with the behavior of an instability-generated structure.

Numerical simulations of the experiment were conducted using the code RAPTOR, a three-dimensional Eulerian adaptive mesh refinement (AMR) code that uses a higher-order Godunov method applied to the volume-of-fluid description of the multifluid equations of gas dynamics [8–10]. Several different equation-of-state formulations have been used to describe the target materials, with little difference in the results. The calculations were run on a 32-node cluster of Digital/Compaq ES40's, with each node containing four 667 MHz EV67 CPU's.

Several approximations are made in the simulations. Electron conduction and radiation transport effects are not included, as these are negligible once the incident shock is launched into the plastic. The slightly curved incident shock is approximated as being planar, and the Be tube is not included. Only one quadrant of the experiment is simulated. Even with this restricted problem, the calculation contained just over 20×10^6 cells on the finest level of refinement at 39 ns. The multimode surface finish of the Cu sphere was included with an rms perturbation comparable to that of the experimental target. Testing showed that the evolution of the shocked sphere was relatively insensitive to the initial perturbation spectrum, however.

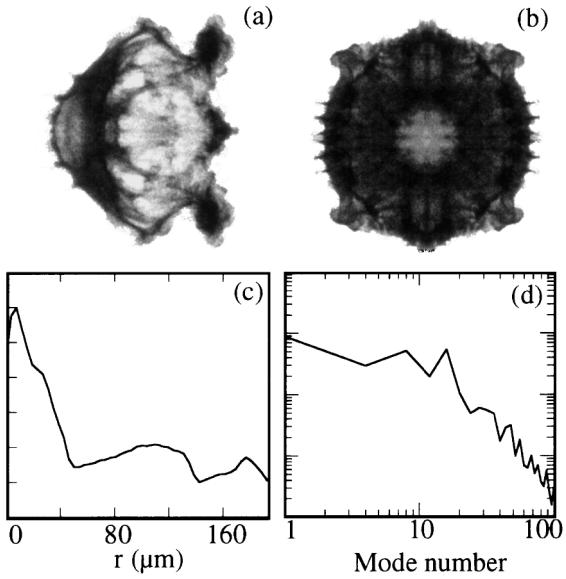

FIG. 4. (a) Side-on and (b) face-on radiographs from the 3D numerical simulation. (c) Radial lineout through the face-on image of (b). (d) Mode number spectrum of the azimuthal lineout through the face-on image of (b).

Radiographs of the numerical simulations are shown in Figs. 4(a) and 4(b) for $t = 39$ ns. The simulated radiographs reproduce all the key experimentally observed features. Namely, the inner and outer rings are evident in the simulated face-on radiograph as well as the appearance of an azimuthal modulation. The two-ring structure is quantified in Fig. 4(c) using the same procedure as was used to produce Fig. 3(b). The central transparent region is again seen as well as the inner and outer rings at $r = 45$ and 140 μm, respectively. The azimuthal mode number spectrum for the outer ring, determined in the same manner as that of Fig. 3(f), is shown in Fig. 4(d). A peak is seen at a mode number of approximately 15 in agreement with the experimental observations. Further details of the numerical simulations together with a more complete description of the AMR code will be given in a future report.

In the work of Widnall, Bliss, and Tsai [11], a theory was developed for the azimuthal instability of a vortex ring. This theory provides the growth rate of an azimuthal mode as a function of the nondimensional translational velocity of the ring, $V = \ln(8R/a) - 1/4$, which is a function of the ratio of the mean ring radius R to the vortex core radius a. This ratio can be quantitatively estimated from our experimental radiographs. From Fig. 3(b), the width of both the inner and outer rings is seen to be approximately 40 μm giving a core radius of 20 μm. For the outer ring, the radius is 127 μm. Using the theoretical results of Widnall *et al.,* this corresponds to a nondimensional translational velocity of 3.67 which suggests an unstable mode of $n = 15$–17 depending on whether the distribution of the vorticity in the vortex ring is constant or nonuniform. This estimate agrees remarkably well with the results of both the experiment and numerical simulations. For the inner ring, the ring radius is 47 μm corresponding to a translational velocity of 2.67. From [11] we get $n = 5$–7 for the dominant mode. Again this compares remarkably well with the experimentally determined value of $n = 5$.

The results presented here are significant in the following three regards. First, while this interaction has been experimentally studied in the past at both a low and a high Mach number, the present experimental results are the first to diagnose the three-dimensional structure of this flow. Second, these experimental results provide a rigorous and quantitative validation test of any numerical simulation. Two-dimensional codes are completely inadequate, as the azimuthal instability is inherently three dimensional. The appearance of a single dominant azimuthal mode number in the experiment arising from a broadband initial perturbation provides a quantitative measure of the agreement between experiment and simulation. Finally, the observation that an incompressible theory describing the instability of a much simpler structure (a single vortex ring) applies to the present problem is of great importance in that it extends the applicability of the incompressible theory far beyond its originally intended range of validity. This allows us to now quantitatively predict many aspects of the three-dimensional breakup of localized perturbations.

This work was performed under the auspices of the U.S. Department of Energy by the University of California, Lawrence Livermore National Laboratory under Contract No. W-7405-Eng-48.

[1] R. I. Klein, C. F. McKee, and P. Colella, Astrophys. J. **420**, 213 (1994).
[2] R. I. Klein and C. F. McKee, *Numerical Simulations in Astrophysics* (Cambridge University Press, Cambridge, England, 1994), p. 251.
[3] J.-F. Haas and B. Sturtevant, J. Fluid Mech. **181**, 41 (1987).
[4] R. I. Klein, K. S. Budil, T. S. Perry, and D. R. Bach, Astrophys. J. Suppl. Ser. **127**, 379 (2000).
[5] J. M. Soures *et al.*, Phys. Plasmas **3**, 2108 (1996).
[6] M. Temporal *et al.*, Nucl. Instrum. Methods Phys. Res., Sect. A, **415**, 668 (1998).
[7] K. S. Budil, T. S. Perry, P. M. Bell, J. D. Hares, P. L. Miller, T. A. Peyser, R. Wallace, H. Louis, and D. E. Smith, Rev. Sci. Instrum. **67**, 485 (1996).
[8] M. J. Berger and J. Oliger, J. Comput. Phys. **53**, 484 (1984).
[9] M. J. Berger and P. Colella, J. Comput. Phys. **82**, 64 (1989).
[10] C. A. Rendleman, V. E. Becker, M. Lijewski, W. Y. Crutchfield, and J. B. Bell, Comput. Visualization Sci. **3**, 147 (2000).
[11] S. E. Widnall, D. B. Bliss, and C. Tsai, J. Fluid Mech. **66**, 35 (1974).